Instability of SPH applied to Poiseuille flow

Baofang Song[a,*], Arman Pazouki[b], Thorsten Pöschel[a]

[a] *Institute for Multiscale Simulation, Friedrich-Alexander-Universität Erlangen-Nürnberg, Nägelsbachstraße 49b, 91052 Erlangen, Germany*
[b] *Department of Mechanical Engineering, University of Wisconsin-Madison, Madison, WI 53706-1572, USA*

Abstract

Weakly compressible smoothed particle hydrodynamics (WCSPH) has been widely applied to flows with free surfaces, multi-phase flow and systems with complex boundary geometry. It is known, however, that WCSPH suffers from transverse instability when applied to simple wall-bounded shear flows such as Poiseuille and Couette flows at moderate and high Reynolds number, $\mathrm{Re} \gtrsim 1$, casting the application of WCSPH to practical situations into doubt, where the Reynolds number is frequently large. Here, we consider Poiseuille flow for a wide range of Reynolds number and find that the instability of WCSPH can be avoided by using appropriate ratio of smoothing length to particle spacing in combination with a density re-initialization technique. We also probe the source of the instability and point out the limitations of WCSPH for wall-bounded shear flows at high Reynolds number.

Keywords: weakly compressible smoothed particle hydrodynamics, transverse instability, smoothing length to particle spacing ratio, density re-initialization, wall-bounded shear flow

1. Introduction

Originally, *smoothed particle hydrodynamics* (SPH) was proposed to solve astrophysical problems [1, 2], however, by now there is a much wider range of application. Because of its meshless and particle-based nature, it is frequently applied to fluid flows with free surfaces [3, 5], multi-phase systems

*Corresponding author
Email address: baofang.song@fau.de (Baofang Song)

[5, 4, 6, 7], and systems with complex boundary geometry [8]. Very recently it was also applied to particle laden flow fully resolving the flow around moving particles [9]. For a comprehensive review on the fundamentals and applications of SPH see [10, 11]. Within the SPH paradigm, there are two different approaches to handle incompressible flow problems, namely *truly incompressible SPH* (ISPH) which imposes incompressibility by solving the pressure Poisson equation [5, 12, 13, 14] and *weekly compressible SPH* (WCSPH), which exploits an equation of state to relate density and pressure and approximately imposes the incompressibility by assigning high speed of sound. Mainly because of its computational simplicity, WCSPH was extensively used for various flow simulations, e.g. [3, 4, 5, 8, 15]. In this paper, we focus on its application to incompressible wall-bounded shear flow.

For shear flow at low Reynolds numbers, WCSPH yields satisfactory results, e.g. [8, 9, 15, 16, 20]. However, for larger Reynolds numbers, WCSPH fails, in particular in simulations of simple shear flow. Imaeda & Inutsuka [17] pointed out that in standard SPH the particle velocity cannot exactly represent the fluid velocity, therefore, density error gradually increases and invalidates the simulation results. Similar to a recent transport-velocity formulation for SPH [7], the solution provided in [17] relies on two velocities, i.e. the particle and fluid velocities.

For plane Poiseuille flow, Basa *et al.* [18] investigated the performance of various viscous force formulations and boundary condition implementations in WCSPH and observed failure of the method regardless of the form of viscous force and boundary condition even at a very low Reynolds number, $\mathrm{Re} \approx 1$. The authors identified the inherent inability of WCSPH to suppress transverse fluctuations as the source of the instability, in agreement with earlier studies [16, 19]. The same source of failure was found by Meister *et al.* [20] who considered plane Poiseuille and Couette flows and found divergence of SPH for $\mathrm{Re} \gtrsim 65$. For smaller Reynolds number, the simulation converges, however, the deviation from the analytical solution is considerable ($\approx 10\%$ for $\mathrm{Re} = 65$). It is also concluded that regular initial particle distributions are intrinsically unstable with respect to transverse fluctuations in Poiseuille and Couette flows [20].

The appearance of the instability poses fundamental limitation of the application of SPH to wall-bounded shear flows. In this paper we study the effects of method parameters and initial particle configurations on the performance of SPH for simple shear flow and pipe flow at low Reynolds numbers, $\mathrm{Re} \approx 0.01 \ldots 100$ and encounter the same instability as reported in

[16, 18, 20]. We identify inappropriate choice of the ratio of smoothing length to particle spacing as the source of the instability and propose strategies to achieve satisfactory performance of SPH simulations.

2. SPH Methods

SPH is a Lagrangian approach to solve the Navier-Stokes equations numerically using discrete quasi-particles. The discretization scheme is further elaborated in the following sub-sections.

2.1. Continuity equation

The evolution of density can be formulated using the continuity equation

$$\frac{d\rho}{dt} = -\rho \nabla \cdot \boldsymbol{v}, \tag{1}$$

where ρ and $\boldsymbol{v}$ are the fluid density and velocity, respectively. In the formulation of SPH, Eq. (1) reads

$$\frac{d\rho_a}{dt} = \rho_a \sum_b \frac{m_b}{\rho_b} (\boldsymbol{v}_a - \boldsymbol{v}_b) \cdot \nabla_a W_{ab}, \tag{2}$$

where ρ_a is the density of particle a, m_b is the mass of particle b and ∇_a denotes the derivative with respect to the position $\boldsymbol{r}_a$ of particle a. W is the kernel function, and $W_{ab} \equiv W|_{\boldsymbol{r}=\boldsymbol{r}_a-\boldsymbol{r}_b}$. In this paper, the cubic spline kernel function given in [9] with a compact support is employed. Alternatively, the density can also be directly obtained using

$$\rho_a = \sum_b m_b W_{ab}\,. \tag{3}$$

Both types of density updating schemes, Eqs. (2) and (3) yield similar results [18], however, usually the former is preferred as it produces smoother density fields in the vicinity of boundaries [9, 15]. In this paper, we adopt the continuity equation Eq. (2) together with a density re-initialization technique using Eq. (3) [5, 9].

2.2. Momentum equation

The momentum equation reads

$$\frac{d\boldsymbol{v}}{dt} = -\frac{1}{\rho}\nabla p + \frac{\mu}{\rho}\nabla^2\boldsymbol{v} + \boldsymbol{f}, \tag{4}$$

where p is the pressure and $\boldsymbol{f}$ denotes the external body force density. Regarding discretization, we apply the gradient and viscous term formulation given in [6, 8]:

$$\left(-\frac{1}{\rho}\nabla p\right)_a = -\frac{1}{m_a}\sum_b (V_a^2 + V_b^2)\tilde{p}_{ab}\nabla_a W_{ab}\,, \tag{5}$$

$$\left(\frac{\mu}{\rho}\nabla^2\boldsymbol{v}\right)_a = \frac{1}{m_a}\sum_b (V_a^2 + V_b^2)\tilde{\mu}_{ab}\frac{\boldsymbol{r}_{ab}\cdot\nabla_a W_{ab}}{|\boldsymbol{r}_{ab}|^2 + \epsilon h^2}(\boldsymbol{v}_a - \boldsymbol{v}_b)\,, \tag{6}$$

where $V_a \equiv m_a/\rho_a$ is the volume of particle a,

$$\tilde{p}_{ab} \equiv \frac{\rho_a p_b + \rho_b p_a}{\rho_a + \rho_b} \qquad \text{and} \qquad \tilde{\mu}_{ab} \equiv 2\frac{\mu_a \mu_b}{\mu_a + \mu_b} \tag{7}$$

are the inter-particle-averaged pressure and viscosity associated with particles a and b. The term ϵh^2 in the denominator of Eq. (6), where h is the length scale of the smoothing kernel and ϵ is a small number (usually $\epsilon = 0.01$), is introduced to avoid the singularity when $|\boldsymbol{r}_{ab}| \to 0$.

In our simulations we tested also alternative formulations for the pressure gradient and the viscous term proposed in [9, 15] and no significant difference was observed.

2.3. Equation of state

To relate pressure and density, we use the equation of state [10]

$$p = B\left[\left(\frac{\rho}{\rho_0}\right)^{\gamma} - 1\right], \tag{8}$$

where p is the dynamic pressure and $B \equiv c^2\rho_0/\gamma$, with the numerical speed of sound, c, which should be large compared to the flow speed in order to keep the density variation small. In this paper, c is taken 10 times the maximum velocity of the steady Poiseuille flow. Following [10], we chose $\gamma = 7$. Nevertheless, other values such as $\gamma = 1$ have also been suggested [7, 21].

2.4. No-slip boundary condition

The no-slip boundary condition is achieved by using dummy particles located outside of the flow domain. We chose the implementation proposed in [8] which has been shown robust. The properties of dummy particles are not updated according to Navier-Stokes equations. They are rather updated based on the following procedure: first, the fluid velocity is extrapolated to the position of wall dummy particles to obtain $\hat{\boldsymbol{v}}$, then the dummy particle velocity is calculated via

$$\boldsymbol{v} = 2\boldsymbol{v}_{\text{wall}} - \hat{\boldsymbol{v}}\,. \tag{9}$$

The pressure of the dummy particles is directly extrapolated from the ambient fluid, and finally the density of dummy particles is calculated according to the equation of state, Eq. (8). For the update of density using Eq. (2), the actual wall velocity, $\boldsymbol{v}_{\text{wall}}$, is assigned to the dummy particles instead of using Eq. (9), see [8].

The problem with this boundary condition is that the position of the wall surface in simulation where $\boldsymbol{v} = 0$ may not coincide with the physical wall surface as it will be determined by the velocity extrapolation and may vary in time, depending on the particle distribution near the wall. While this problem is inherent to the modeling, its effect can be reduced by increasing the spatial resolution. Further numerical errors appear due to the boundary pressure approximation in the region near the wall. Since an accurate wall boundary formulation for SPH is still lacking, all SPH simulations are affected by these problems, however, their significance may depend on the specific application and on the details of the model.

3. Failure of SPH applied to plane Poiseuille flow

Using the method described in the previous Section, we simulate plane Poiseuille flow in three dimensions with periodic boundary condition in the flow direction and spanwise direction. Initially the flow is at rest and driven by a constant body force (e.g. gravity). The system is integrated in time using a 2^{nd}-order Runge-Kutta scheme [9]. The Reynolds number is defined as $\text{Re} = Hv_{\max}/2\nu$ where H is the channel gap width, $\nu = \mu/\rho_0$ is the kinematic viscosity of the fluid, and $v_{\max}$ is the characteristic velocity. Herein $v_{\max}$ is the maximum velocity of the steady Poiseuille flow. In all following tests, we chose the reference density $\rho_0 = 1000\,\text{kg/m}^3$, $\nu = 10^{-4}\,\text{m}^2/\text{s}$ and $H = 0.2\,\text{m}$. We vary the body force density, f, to vary the terminal velocity

and, thus, the terminal Reynolds number assumed for $t \to \infty$. The numerical results are compared with the analytical solution of the transient Poiseuille flow under constant body force [15]. Using the described geometry and viscosity, the analytical solution will assume its steady state, i.e., the parabolic laminar flow profile, at time $t \gtrsim 240\,\mathrm{s}$.

We simulate plane Poiseuille flow using SPH for three values of the Reynolds number, $\mathrm{Re} = \{0.06, 6, 120\}$. Here and in the following the value of Re indicates the Reynolds number of the asymptotic velocity profile due to the chosen body force density. The lowest value, $\mathrm{Re} = 0.06$, corresponds to $f = 1.2 \times 10^{-6}\,\mathrm{m/s^2}$ leading to an asymptotic flow with peak velocity at the channel center $v_{\max} = 6 \times 10^{-5}\,\mathrm{m/s}$ and bulk velocity $U = \frac{2}{3} v_{\max} = 4 \times 10^{-5}\,\mathrm{m/s}$. We distribute 40 particles across the channel width corresponding to particle spacing ratio $\Delta x = 0.005\,\mathrm{m}$. For the smoothing length, being the characteristic length scale associated with the kernel function we chose $h = 0.005\,\mathrm{m}$. Thus, the characteristic ratio of the smoothing length over the particle spacing assumes the value $h/\Delta x = 1$. Figure 1a shows the velocity profiles due to the numerical and analytical solutions.

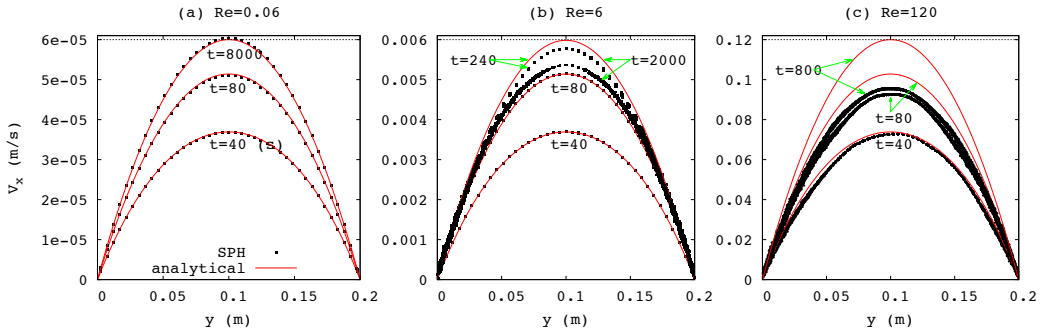

Figure 1: Velocity profiles of plane Poiseuille flow for $\mathrm{Re} = 0.06$ (a), $\mathrm{Re} = 6$ (b) and $\mathrm{Re} = 120$ (c) at different time, t, starting at rest at $t = 0$. Lines: analytical solution; symbols: simulation result.

At this low Reynolds number, for all times the simulation results agree, up to good accuracy, with the transient analytical solutions. The largest time, $t = 8,000\,\mathrm{s}$ (corresponding to $2.4H/v_{\max}$), is plotted against the stationary

solution. The accuracy may be quantified by means of the L_2 norm

$$L_2 = \sqrt{\frac{\sum\limits_{\{N\}} \left[v_x - U_x\left(\boldsymbol{r}\right)\right]^2 + v_y^2 + v_z^2}{\sum\limits_{\{N\}} U_x\left(\boldsymbol{r}\right)}}, \tag{10}$$

where $\boldsymbol{v} = (v_x, v_y, v_z)$ are the velocity components in the streamwise, wall normal and spanwise directions, and $U_x\left(\boldsymbol{r}\right)$ is the analytical streamwise velocity at the (particle) position $\boldsymbol{r}$. The summation is performed over all N fluid particles at positions $\boldsymbol{r}$ traveling at of velocity $\boldsymbol{v}$. The stationary solution for $\mathrm{Re} = 0.06$ shown in Fig. 1a corresponds to $L_2 = 0.8\%$.

For intermediate Reynolds number, $\mathrm{Re} = 6$, we use the parameters $h = 0.005\,\mathrm{m}$, $h/\Delta x = 1$, and $f = 1.2 \times 10^{-4}\,\mathrm{ms}^{-2}$. Figure 1b shows the corresponding profiles of the velocity obtained from the simulation in comparison with the analytical result. Again, at $t = 0$ the flow starts at rest. For short time, when velocity is far below the asymptotic value, analytical and numerical velocity profiles agree well. For larger time, $t = 240\,\mathrm{s}$, when the analytical solution converged to the stationary state, however, large deviations between the analytical and numerical solutions appear. For yet larger time, the SPH solution deviates further from the analytical steady state solution and seems to converge to a blunted velocity profile at about $t = 2000\,\mathrm{s}$.

Besides that, we also observed a characteristic evolution of the fluctuations of the velocity profile: the velocity field first becomes noisy near the walls; later the noise spreads out from the near wall region to almost the entire flow domain. This is different from the case $Re = 0.06$, see Fig. 1a, where the particles stay aligned in rows during the entire simulation. We believe that the inaccurate wall boundary condition introduces perturbations of the velocity field near the wall and cause particles to undergo transverse drift. Under shear, the (cross-shear) transverse drift of particles might cause inhomogeneity of the particle distribution and undermine the smoothing of SPH. [18]. This effect is not observed at $Re = 0.06$ because the perturbations are negligible at very low Reynolds numbers. We conjecture that both observations are related and that the perturbations of the velocity profile causes deviation of the numerical velocity profile from the analytical one for larger flow velocity. At $t = 2000\,\mathrm{s}$, the L_2-error reaches 10%, which is unacceptably large. We wish to point out that the described effects: noisy flow field, blunted velocity profile, and large L_2 in the stationary state, are not the effects of turbulence since the Reynolds number is far lower than the lowest

Reynolds number at which turbulence can be observed in plane Poiseuille flow (about 800 [22]).

Poiseuille flow at high Reynolds numbers is rarely discussed in the literature. Here we perform simulations for Re = 120. The parameters are $f = 2.4 \times 10^{-3}\,\mathrm{ms}^{-2}$, $h = 0.004\,\mathrm{m}$, and $h/\Delta x = 1$. It is known that SPH simulations fail at large Reynolds number [18, 20] which is in agreement with our simulation shown in Fig. 1c. Here we observe large deviations between analytical and numerical simulations even for $t = 40\,\mathrm{s}$, including large noise, asymmetry of the velocity profile and a non-physical plateau at the channel center becomes apparent. Obviously, for Re = 120 SPH cannot be applied to simulate Poiseuille flow.

The results suggest that WCSPH fails at Reynolds number $\mathrm{Re} \gtrsim 1$, in agreement with [16, 18, 20].

4. The effect of smoothing length, h, smoothing length to particle spacing ratio, $h/\Delta x$, initial particle configuration, and density re-initialization on the stability of the simulation

The failure of WCSPH in plane Poiseuille flow, reported previously [16, 18, 20] and also shown in the previous Section restricts the applicability of the method to systems with very small Reynolds number. In this section, we analyze the sources of the errors and test measures to improve the stability of WCSPH. Naïvely, the accuracy of SPH seems to be determined by the system parameters h and $h/\Delta x$ [23, 24, 25]. As discussed above, the initial particle configuration and density re-initialization are also important. In this section, we investigate the influence of these ingredients in detail.

4.1. Influence of the smoothing length, h

Figure 2 shows the L_2-error, according to Eq. (10), for Re = 6 and Re = 120 using smoothing length $h = \{2, 3, 4, 5\} \times 10^{-3}\,\mathrm{m}$, where $h = 0.002\,\mathrm{m}$ corresponds to 100 particles across the channel width.

For Re = 6, the L_2 value increases perpetually to $L_2 > 10\%$ and no convergence can be seen. For Re = 120 the error converges, however, yet at a higher level, $L_2 \approx 20\%$. For both cases, reducing the smoothing length does not noticeably improve the stability, which is in agreement with [18]. We believe that the smoothing length has only minor influence on the stability, if any.

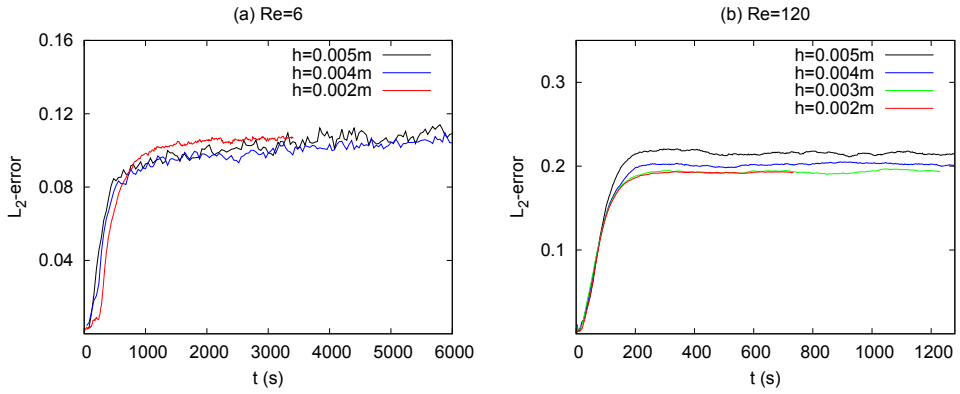

Figure 2: L_2 over time for simulations at Re = 6 (a) and Re = 120 (b) for different smoothing length, h.

4.2. Influence of smoothing length to particle spacing ratio, $h/\Delta x$

Figure 3 shows L_2 over time for different values of the smoothing length to particle spacing ratio, $h/\Delta x = \{1, 1.3, 1.5\}$, again for Re = 6 and Re = 120. The smoothing length was chosen $h = 0.005\,\mathrm{m}$ for Re = 6 and $h = 0.004\,\mathrm{m}$ for Re = 120. We observe drastic reduction of the L_2-error with increasing

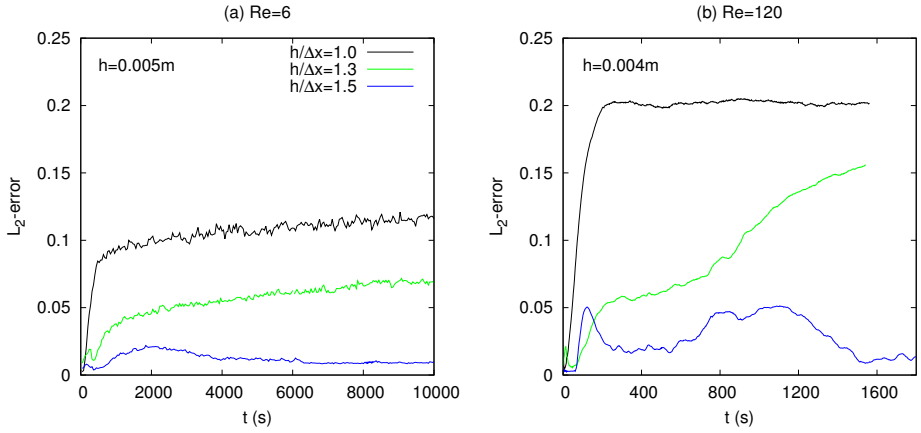

Figure 3: L_2 over time for simulations at Re = 6 (a) and Re = 120 (b) for different smoothing length to particle spacing ratio, $h/\Delta x$.

$h/\Delta x$ for both cases, Re $= 6$ and Re $= 120$. While for $h/\Delta x = 1$ and $h/\Delta x = 1.3$ the error is still unacceptably large and possibly diverges, for $h/\Delta x = 1.5$ we obtain $L_2 < 2\%$ in the entire time domain for Re $= 6$ and $L_2 < 5\%$ for Re $= 120$. The significant influence of $h/\Delta x$ for Poiseuille flow agrees with earlier results by Ellero and Adams [24], who computed the friction forces acting on a cylinder confined in channel flow using SPH and found $h/\Delta x \gtrsim 1.5$ necessary for stable converging results.

4.3. Influence of the initial particle distribution

In many SPH simulations, the initial particle positions are chosen regularly, e.g. located on a rectangular or triangular lattice. It was mentioned, however, that this choice of initial conditions may contribute to instability of the numerical solution [18, 20]. In order to investigate the influence of the initial conditions, we compare the numerical results obtained using initial positions where the particles start at rest from a rectangular lattice with the results using irregular initial conditions. The irregular particle setup is generated in the following way: particles start from lattice positions but at random velocity, then the system is relaxed by solving the Navier-Stokes equations in the absence of the external body force until the maximum velocity in the domain is below 10^{-9} m/s, implying an equilibrium state. Figure 4 shows L_2 over time for regular and irregular initial conditions for $Re = 120$.

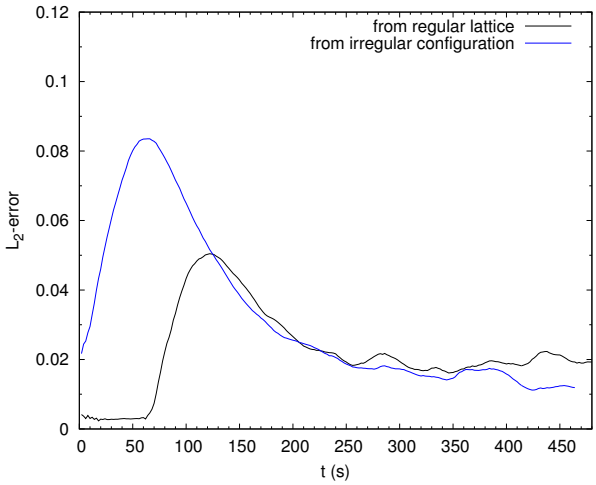

Figure 4: L_2 over time for Poiseuille flow at $Re = 120$ for regular and irregular initial conditions. Other parameters are $h = 0.004\,\mathrm{m}$ and $h/\Delta x = 1.5$.

As expected, both simulations lead to identical stationary states, that is, the same L_2 value up to fluctuations. The accuracy of the transient flow is, however, better for the case of regular initial positions, thus, we cannot confirm the argument presented in [18, 20].

4.4. Influence of density re-initialization

Updating density via the continuity equation via Eq. (3) instead of the direct density summation via Eq. (2) imposes an inconsistency of mass, density and the volume occupied by the particles [5, 15]. Morris *et al.* [15] pointed out that this is not important for flow at low Reynolds number (see also our results at $Re = 0.06$), however, at larger Reynolds number, this inconsistency may lead to a noisy flow field and inaccurate results [5]. Considerable improvement could be achieved using the density re-initialization technique [5]. This technique aims to improve the density field obtained from Eq. (2) by frequently using the direct density summation in Eq. (3). This involves a summation over all particles and increases the computation costs. Fortunately this correction only needs to be performed at a much lower frequency than the time-stepping. Usually this technique is performed every 10 or 20 time steps [5, 9, 20]. Colagrossi *et al.* [5] tested the effects of the re-initialization frequency and showed that a frequency around 20 shows a good performance in terms of total kinetic energy conservation.

Figure 5a shows the deviation of the simulation result from the analytical solution quantified by L_2 for Re = 120 ($h = 0.004\,\mathrm{m}$, $h/\Delta x = 1.5$) when applying the density re-initialization technique together with the zeroth order correction of the density summation [9, 20], which is important near solid boundaries, where the support of fluid particles is incomplete.

We find that density re-initialization reduces L_2 by almost an order of magnitude to $L_2 < 1\%$ for the entire simulation. Moreover, the stationary velocity profile obtained from SPH agrees well with the analytical solution, Fig. 5b. For further evaluation, Fig. 6a shows the fluctuations of density, revealing a reduction of almost an order of magnitude when applying density re-initialization. Similarly, the fluctuations of pressure are reduced as well. As shown in Fig. 6b, evidently due to the relation between pressure and density given by the equation of state in WCSPH. Finally, Figs. 6c,d show the transverse velocity fluctuations in the flow domain, which illustrates the regularization of the velocity field due to applying the density re-initialization technique. Choosing the numerical speed of sound to be 10 times the maximum flow velocity ($0.12\,\mathrm{m/s}$), the density variation obtained from the simu-

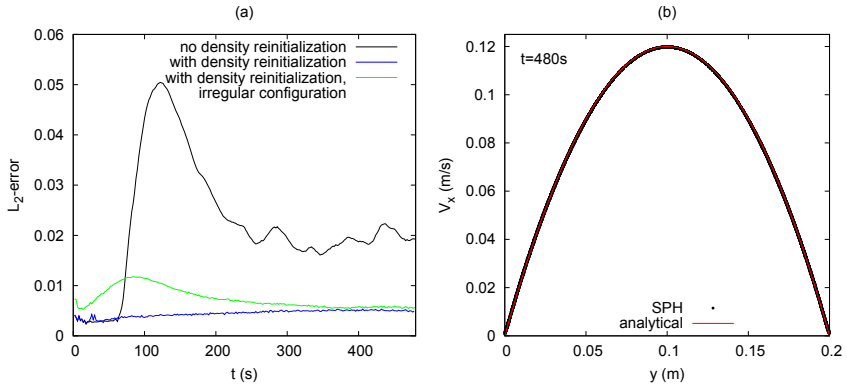

Figure 5: (a) L_2 over time for simulations of Poiseuille flow $Re = 120$ with and without density re-initialization. (b) Velocity profiles at $t = 480\,\mathrm{s}$ obtained from SPH ($h = 0.004\,\mathrm{m}$, $h/\Delta x = 1.5$, density re-initialization) in comparison with the analytical solution.

lation without density re-initialization is below 1%. However, the transverse velocity fluctuations close to the wall boundary can reach about 1.7% of the centerline velocity. Density re-initialization reduces the velocity fluctuations. Nevertheless, this effect is only significant far from the wall where the fluctuations almost vanish, see Fig. 6c,d. Velocity fluctuations near the wall boundary are not significantly reduced which is due to the fact that they are rooted in the inaccurate boundary velocity and pressure approximation.

As explained in Sec. 2.4, the velocity boundary condition implementation introduces fluctuations to the wall position which depend on the particle distribution near the wall which in turn leads to perturbations of the flow. Moreover, the boundary pressure approximation also generates additional velocity disturbances near the wall. These two factors add up and influence the flow in a similar manner as a rough wall. Following this picture, disturbances of the flow originate from the wall and propagate from there. At low Reynolds numbers, these fluctuations are small and spread very slowly. Consequently SPH was found to give accurate result at very low Reynolds number in the literature. However, as Re increases, the disturbances arising from the wall become larger and spread faster to other flow regions, which results in a noisy flow field. This seems to be the main source of transverse disturbances, which cause inhomogeneous particle distrubution and reduce the accuracy of SPH, called transverse instability [18, 20]. This effect is par-

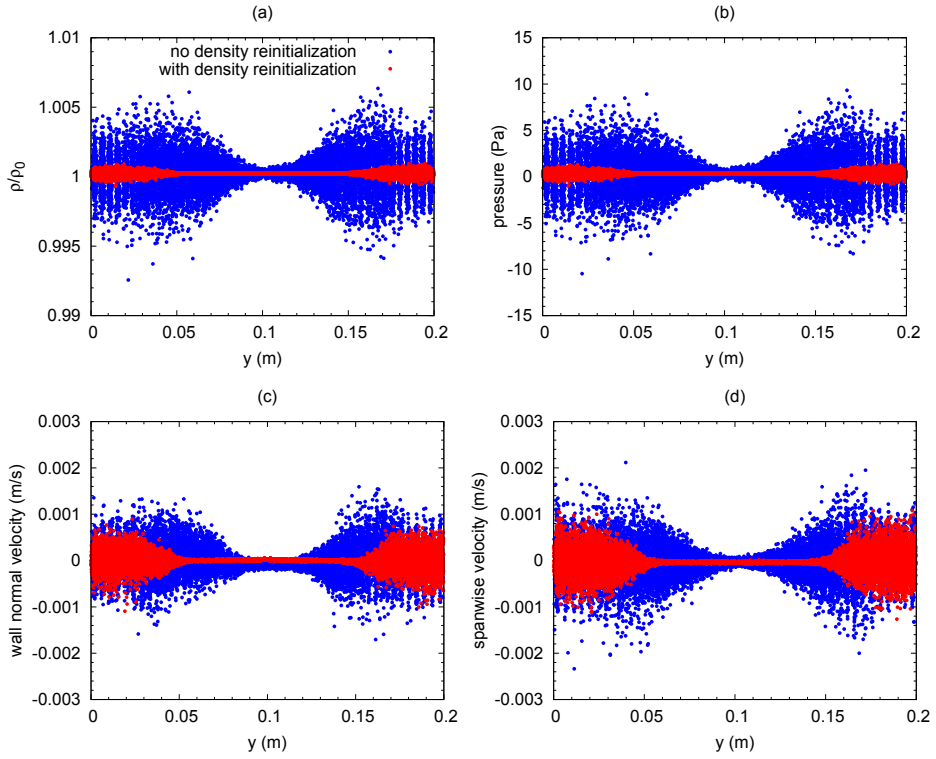

Figure 6: Comparison of the simulation results with and without density re-initialization for $Re = 120$. (a) Density normalized by the reference density $\rho_0 = 1000\,\mathrm{kg/m^3}$; (b) pressure; (c) velocity normal to the wall; (d) spanwise velocity. Parameters are $h = 0.004\,\mathrm{m}$, $h/\Delta x = 1.5$, data are taken at $t = 120\,\mathrm{s}$ when the difference of the L_2 values is maximal, see Fig. 5a.

ticularly significant in flows where the wall-shear dominates the flow state, such as simple wall-bounded shear flow. Our simulations show that this instability can be largely suppressed by choosing proper system parameter $h/\Delta x$ and the density re-initialization technique.

5. Pipe flow

In order to demonstrate that the above arguments are relevant for other wall-shear flows too, herein we study the influence of the smoothing length to particle spacing ratio, $h/\Delta x$, and the density re-initialization scheme for pipe flow at Re = 120 which is much larger than usual test cases reported

in the literature. The Reynolds number is defined as $\mathrm{Re} = UD/\nu$ where U and D are the mean flow speed and pipe diameter, respectively. We assume the following parameters: $D = 0.2\,\mathrm{m}$, $\rho_0 = 1000\,\mathrm{kg/m^3}$, $\nu = 10^{-4}\,\mathrm{m^2/s}$, pipe length $L = 0.06\,\mathrm{m}$ and the constant driving body force density $f = 4.8 \times 10^{-3}\,\mathrm{ms^{-2}}$. The corresponding stationary Hagen-Poiseuille flow with parabolic velocity profile has a peak velocity of $0.12\,\mathrm{m/s}$ at the center of the pipe. To model the pipe geometry, we distribute particles on a lattice in a rectangular box and mark particles inside the circular pipe as fluid particles and the rest as wall particles. We only keep wall particles that are within a distance about 3 times the average particle spacing from the pipe wall and use them to impose the no-slip boundary condition at the wall. We choose $h = 0.004\,\mathrm{m}$ and investigate the effect of density re-initialization and spacing ratio for $h/\Delta x = 1.0$ and and $h/\Delta x = 1.5$.

Figure 7a shows the L_2 according to Eq. (10) with the analytical so-

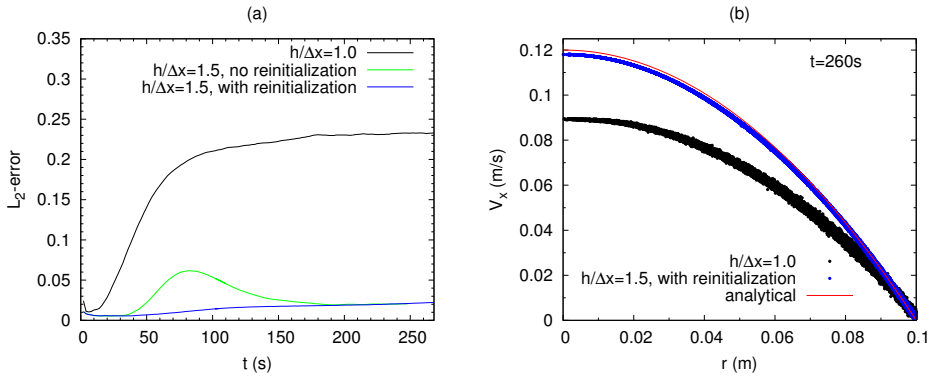

Figure 7: SPH simulation of pipe flow under constant driving body force at $\mathrm{Re} = 120$. (a) L_2 over time time for $h/\Delta x = \{1, 1.5\}$ with and without density re-initialization. (b) Velocity profile at time $t = 260\,\mathrm{s}$ obtained from the SPH simulation in comparison with the analytical result [16]. The simulation result with and without density re-initialization coincide up to line width.

lution given in Ref. [16] over time, for different values of $h/\Delta x$, with and without density re-initialization. Similar to Poiseuille flow, we obtain great improvement of the quality of the numerical solutions, expressed by considerable reduction in L_2 when increasing $h/\Delta x$ from 1 to 1.5. Considering the results for $h/\Delta x = 1.5$ (green line in Fig. 7a) we observe a non-monotonous evolution of L_2 which grows up to 7%. This implies the accuracy of the tran-

sient solution is clearly worse than the accuracy of the stationary solution which agrees up to $L_2 = 2\%$ with the analytical result. The inability to accurately capture the transient flow is a severe drawback of standard SPH. This problem can be suppressed using the density re-initialization technique

Similar improvement of the simulation result can be seen in Fig. 7b, where the velocity profile at time $t = 260\,\mathrm{s}$ (corresponding to 80 convective time units D/U) is shown. Increasing $h/\Delta x$ and using density re-initialization does not only yield a velocity profile much closer to the analytical solution but also reduces the noise level significantly.

The deviation of the stationary velocity profile obtained from SPH from the analytical solution, expressed by a finite L_2 value for large time (see Fig. 7a) is partially due to the imperfect modeling of the cylindrical boundary described before. In fact, due to our modeling, the computational domain used for SPH is a pipe with small streamwise groove-like structures with characteristic height and azimuthal separation of about Δx. This roughness perturbs the flow and contributes to the noisy flow field in particular close to the wall boundary; see the broad distribution of the streamwise velocity of particles close to the boundary $r = 0.1\,\mathrm{m}$ in Fig. 7b.

Again, we point out that these velocity fluctuations are certainly not due to turbulence since the system operates in a regime far below the lowest Reynolds number at which turbulence can be observed in pipe flow ($\mathrm{Re} \approx 1760$ [26]).

The results presented in this section show that without careful parameter choice and the density re-initialization SPH fails for the simulation of pipe flow at low Reynolds number, $\mathrm{Re} = 120$, just in the same way and due to the same reasons as for plane Poiseuille flow discussed in Sec. 4.

6. Conclusion

We investigated the stability of WCSPH simulations for the example of Poiseuille flow with respect to smoothing length h, smoothing length to particle spacing ratio $h/\Delta x$, initial setup of the fluid particles, and density re-initialization. The accuracy of the simulation results was quantified by evaluating the deviation of the numerical flow velocity field from the analytical solution at late time when the stationary regime is assumed and by the L_2 norm as a function of time, characterizing the deviation of the entire flow field as obtained from the SPH simulation from the transient analytical solution.

In agreement with the literature [16, 18, 19, 20] we found that SPH delivers quantitatively precise results only for the case of very small Reynolds number, e.g., Re = 0.06 while it fails dramatically for larger Reynolds number. Reducing the smoothing length, h, does not improve the stability of the simulation. However, increasing $h/\Delta x$ for fixed value of h strongly improves the results. For our setup we found that $h/\Delta x \gtrsim 1.5$ is necessary to obtain reliable results for Poiseuille flows at moderate and high Reynolds number ($Re \gtrsim 1$). This requirement considerably increases the computational costs since the smoothing length to particle spacing ratio affects the size of particles neighbor list. For our system, in contradiction to [20], the choice of irregular initial particle positions leads to significantly larger error than regular initial positions, in particular during the transient time, while the asymptotic velocity profile was not affected by the initial particle positions. We also showed that density re-initialization is necessary for WCSPH that adopts continuity equation for density update, except for very small Reynolds number. This technique reduces density, pressure, and velocity fluctuations in the flow domain, especially in regions far from the wall boundary.

When modeling the domain boundary by means of dummy SPH particles, the boundary velocity and the boundary pressure approximation introduces additional velocity disturbances near the wall. The disturbances gradually propagate to the entire domain, resulting in noisy fields of flow velocity and other hydrodynamic fields. Evidently, modeling the boundaries with discrete particles does not allow for the description of perfectly smooth and impermeable walls. The resulting irregularity due to this approach may be understood as a certain roughness which in turn may be quantified through the specific boundary condition implementation and the corresponding parameters. We believe that a quantitative description of this *numerical* roughness would allow to apply SPH for simulations of fluid flow in the vicinity of *physically* rough walls, which is subject of current research.

Acknowledgement

We thank the German Research Foundation (DFG) for funding through the Cluster of Excellence "Engineering of Advanced Materials". The authors would like to thank Professor Dan Negrut for his comments on a draft of this manuscript.

References

[1] Lucy, L. B. A numerical approach to the testing of the fission hypothesis. *Astron. J.* **82**, 1013-24 (1977).

[2] Gingold, R. A. & Monaghan, J. J., Smoothed particle hydrodynamics: theory and application to non-spherical stars. *Mon. Not. R. Astron. Soc.* **181**, 375-89 (1977).

[3] Monaghan, J. J. Simulating free surface flows with SPH. *J. Comput. Phys.* **110**, 399-406 (1994).

[4] Morris, J. P. Simulating surface tension with smoothed particle hydrodynamics. *Int. J. Numer. Meth. Fluids* **33**, 333-353 (2000).

[5] Colagrossi, A. & Landrini, M. Numerical simulation of interfacial flows by smoothed particle hydrodynamics. *J. Comput. Phys.* **191**, 448-475 (2003).

[6] Hu, X. Y. & Adams, N. A. An incompressible multi-phase SPH method. *J. Comput. Phys.* **227**, 264-278 (2007).

[7] Adami, S., Hu, X. Y. & Adams, N. A. A transport-velocity formulation for smoothed particle hydrodynamics. *J. Comput. Phys.* **241**, 292-307 (2013).

[8] Adami, S., Hu, X. Y. & Adams, N. A. A generalized wall boundary condition for smoothed particle hydrodynamics. *J. Comput. Phys.* **231**, 7057-7075 (2012).

[9] Pazouki, A. & Negrut, D., A numerical study of the effect of particle properties on the radial distribution of suspensions in pipe flow. *Computers & Fluids* **108**, 1-12 (2014).

[10] Monaghan, J. J. Smoothed particle hydrodynamics. *Rep. Prog. Phys.* **68**, 1703-1759 (2005).

[11] Liu, M. B. & Liu, G. R. Smoothed particle hydrodynamics (SPH): an overview and recent developments. *Arch Comput Methods Eng* **17**, 25-76 (2010).

[12] Cummins, S. J. & Rudman, M. An SPH projection method. *J. Comput. Phys.* **152**, 584-607 (1999).

[13] Hu, X. Y. & Adams, N. A. An incompressible multi-phase SPH method. *J. Comput. Phys.* **227**, 264-278 (2007).

[14] Xu, R., Stansby, P. & Laurence, D. Accuracy and stability in incompressible SPH (ISPH) based on the projection method and a new approach. *J. Comput. Phys.* **2009**, 6703-6725 (2009).

[15] Morris, J. P., Fox, P. J. & Zhu, Y. Modeling low Reynolds number incompressible flows using SPH. *J. Comput. Phys.* **136**, 214-226 (1997).

[16] Sigalott, L. D. G., Klapp, J., Sira, E., Meleán, Y. & Hasmy, A. SPH simulations of time-dependent Poiseuille flow at low Reynolds numbers. *J. Comput. Phys.* **191**, 622-638 (2003).

[17] Imaeda, Y. & Inutsuka, S.-I. Shear flows in smoothed particle hydrodynamics. *Astrophys. J.* **569**, 501-518 (2014).

[18] Basa, M., Quinlan, N. J. & Lastiwka, M. Robustness and accuracy of SPH formulations for viscous flow. *Int. J. Numer. Meth. Fluids* **60**, 1127-1148 (2009).

[19] Watkins, S. J., Bhattal, A. S., Francis, N., Turner, J. A. & Whitworth, A. P. A new prescription for viscosity in Smoothed Particle Hydrodynamics. *Astron. Astrophys. Suppl. Ser.* **119**, 177-187 (1996).

[20] Meister, M., Burger, G. & Rauch, W. On the Reynolds number sensitivity of smoothed particle hydrodynamics. *Journal of Hydraulic Research* **52**, 824-835 (2014).

[21] Tamamidis, P.,Zhang, G. & Assanis, D. N. Comparison of pressure-based and artificial compressibility methods for solving three-dimensional steady incompressible viscous flows. *J. Comput. Phys.* **124**, 1 (1996).

[22] Tuckerman, L. S.,Kreilos, T., Schrobsdorff, H., Schneider, T. M. & Gibson, J. F. Turbulent-laminar patterns in plane Poiseuille flow. *Phys. Fluids* **26**, 114103 (2014).

[23] Quinlan, N. J. & Lastiwka, M. Truncation error in mesh-free particle methods. *Int. J. Numer. Meth. Fluids* **66**, 2064-2085 (2006).

[24] Ellero, M. & Adams, N. A. SPH simulations of flow around a periodic array of cylinders confined in a channel. *Int. J. Numer. Meth. Engng* **86**, 1027-1040 (2011).

[25] Koumoutsakos, P. Multiscale flow simulations using particles. *Annu. Rev. Fluid Mech.* **37**, 457-87 (2005).

[26] Kerswell, R. R. Recent progress in understanding the transition to turbulence in a pipe. *Nonlinearity* **18**, R17-R44 (2005).